Correlation between crystallographic superstructure and magnetic structures in finite magnetic fields: A neutron study on a single crystal of Ho_2PdSi_3

Matthias Frontzek,[1,2,*] Fei Tang,[2] Peter Link,[3] Astrid Schneidewind,[2,4] Jens-Uwe Hoffman,[4] Jean-Michel Mignot,[5] and Michael Loewenhaupt[2]

[1]*Neutron Scattering Science Division, Oak Ridge National Laboratory, Oak Ridge, Tennessee 37830, USA*

[2]*Institut für Festkörperphysik, Technische Universität Dresden, D-01062 Dresden, Germany*

[3]*FRM-II, Technische Universität München, D-85747 Garching, Germany*

[4]*Helmholtz-Zentrum Berlin für Materialien und Energie GmbH, D-14109 Berlin, Germany*

[5]*Laboratoire Léon Brillouin, CEA-Saclay, F-91191 Gif-sur-Yvette, France*

(Received 8 July 2010; revised manuscript received 23 September 2010; published 1 November 2010)

We present results of neutron-diffraction experiments on a Ho_2PdSi_3 single crystal in the magnetically ordered state at $T=1.5$ K for magnetic fields applied in the easy $(0,0,L)$ direction. Moderate fields of less than 0.8 T are sufficient to wipe out the antiferromagnetic order in the basal plane of the AlB_2-type hexagonal lattice structure. Concurrently strong magnetic reflections along the $(0,0,L)$ direction develop with increasing fields that are closely related to the nuclear superstructure reflections found in the single crystal at all temperatures. The field dependence of the intensity of these reflections is rather unusual: after a maximum at 0.6 T and a shallow minimum at 2 T a further increase in intensity for fields up to 5 T is observed. A phase transition into a field induced, saturated ferromagnetic state is expected only at very high fields (>13 T) as inferred from magnetization data. For the origin of the high-field magnetic structure two models are proposed and the corresponding model calculations are compared to our experimental results. Furthermore, the experimental data in low fields (<0.8 T) are used to clarify the hitherto unsolved zero-field magnetic structure of Ho_2PdSi_3. The relevance of our findings with respect to other members of the R_2PdSi_3 series (R=Tb, Er, Tm, and others) is emphasized.

DOI: 10.1103/PhysRevB.82.174401 PACS number(s): 75.25.−j

I. INTRODUCTION

The understanding of the magnetic properties and the underlying magnetic structures of the pure rare-earth metals is sometimes cited as the "standard model of rare-earth magnetism."[1] The magnetic behavior and the resulting magnetic structures are explained successfully via a Hamiltonian taking into account the crystal electric field (CEF) effect, the Rudermann-Kittel-Kasuya-Yosida (RKKY) exchange interaction, and the Zeeman term. The oscillatory RKKY exchange dictates the magnetic structure at the ordering temperature T_N which often is an incommensurate magnetic structure since the maximum of $\boldsymbol{J}(\boldsymbol{Q})$ is not bound to the crystallographic structure. These are most often sine-wave-modulated structures, except cases where the in-plane anisotropy is small and helical structure can be stabilized. At lower temperatures the CEF effect promotes commensurate structures. For instance, holmium orders at the Néel temperature ($T_N=132$ K) with a helical structure and is then driven via a lock-in transition to a commensurate structure at 20 K.[1] In the last 30 years a huge number of binary, ternary, and quaternary rare-earth intermetallic compounds have been synthesized and investigated in respect to their magnetic properties and magnetic structures. A good review of the efforts over the last decades has been given by Gignoux and Schmitt.[2]

The magnetic properties in rare-earth intermetallics are often influenced by the competition between incommensurate and commensurate magnetic structures. In phenomenological theories the long-period or incommensurate state is only stable just below T_N.[3] The magnetic ground state at low temperature allows only simple commensurate structures with either ferromagnetic, +− or ++−− sequence of the magnetic moments.[4] The sine-wave modulation is only stable toward low temperatures when the magnetic ground state is a singlet. Otherwise the system undergoes a transition to an equal moment structure.[5,6] If the magnetic system cannot undergo a transition from a sine-wave-modulated magnetic structure to a ferromagnetic order a consequent squaring up of the magnetic structure will occur. This can happen via a first-order transition with a lock in of the propagation vector observed, for instance, in $DyGa_2$ (Ref. 7) or through a continuous transition called progressive squaring up. An example for the latter is $TbCu_2$.[8] However, only few examples of progressive squaring up are known.[5] A rare possibility has been observed in the $CeAl_2$ compound with its Kondo-type behavior.[9] It has been shown that an equal-moment structure minimizes the fourth-order terms in the free energy and therefore promotes a double-$\boldsymbol{\tau}$ structure in this cubic compound.[10] The incommensurate magnetic structure can be described as two equivalent elliptical helices with opposed chirality.[11]

The series of R_2PdSi_3(R=heavy rare-earth) compounds has gone through the phase of initial characterization[12] and elevated interest due to spin-glasslike properties. With the availability of high-quality single crystals[13,14] detailed macroscopic investigations of these properties[15–20] were carried out. The first basic data set for the microscopic understanding has been obtained by magnetic neutron scattering on powder samples.[21] But only neutron-diffraction data on single crystals and their combined interpretation with macroscopic data were the key to the understanding of the more

complex features as recently shown, e.g., for the spin-glasslike magnetic properties of Tb_2PdSi_3 and Er_2PdSi_3.[22] Further, both compounds show a long-range commensurate structures, observed only in a few rare-earth intermetallic compounds such as $PrGa_2$.[23] Also, Er_2PdSi_3 undergoes a progressive squaring up to a noncompensated antiphase structure.

The R_2PdSi_3 compounds crystallize in an AlB_2-derived hexagonal structure ($P6/mmm$). The magnetic rare-earth ions occupy the Al positions while the nonmagnetic Pd and Si atoms were assumed to be statistically distributed on the B positions.[21] The lattice constants are around 4 Å for both ***a*** and ***c*** directions. However, experimental evidence from single-crystal diffraction strongly suggests the presence of Pd-Si order at the B positions.[24]

Additional resolution-limited structural reflections were found on $(m/2,0,n/8)$, $(0,m/2,n/8)$, and $(m/2,m/2,n/8)$ positions with n and m as integers. The Pd-Si order leads to a doubled lattice constant a with Pd_2Si_6 layers. The superstructure of the R_2PdSi_3 compounds is formed by the stacking sequence of these layers which repeats itself every eight layer in ***c*** direction. The direct consequence is the occurrence of two different possible local environments for the rare-earth ions, denoted by $R1$ and $R2$ in the following. The different rare-earth positions have either two or four Pd ions as next-nearest neighbors. The hexagonal symmetry is lost for both positions. The sequences of the local environments of rare-earth ions ($R1$-$R2$-$R2$-$R1$-$R1$-$R1$-$R2$-$R2$) in each layer are predetermined by the Pd-Si order. The rare-earth ions are assumed to remain on their primitive position. For the discussion of the magnetic structure only the facts of two different rare-earth sites and their specific sequence ($R1$-$R2$-$R2$-$R1$-$R1$-$R1$-$R2$-$R2$) is used. A detailed x-ray diffraction study, including extended x-ray-absorption fine structure data and group-theory analysis, in which a model of crystallographic (super)structure is derived, will be published elsewhere.[25]

Most of the R_2PdSi_3 (R=Ce,Gd,Tb,Dy,Ho,Er,Tm) compounds order antiferromagnetically below Néel temperatures comprised between 1.8 K (Tm) and 23.6 K (Tb).[18,20,21,26] Nd_2PdSi_3 orders ferromagnetically below T_C =17 K.[21] De Gennes scaling is not obeyed. Ho_2PdSi_3 has a Néel temperature of 7.7 K.[20] At T_2=2.3 K a second phase transition is observed. In the paramagnetic region (above 50 K) the magnetic easy direction is the $(H,0,0)$ direction in the basal plane. [The difference between real-space directions, e.g., [2, 1, 0], and the corresponding reciprocal lattice vector, e.g., (1, 0, 0), in hexagonal systems often leads to confusion. To prevent this we use the reciprocal directions throughout the paper.] But the magnetic hard-/easy-axis changes around 50 K and in the ordered state the $(0,0,L)$ direction is the magnetic easy direction.[20] The change in anisotropy can be described with higher-order parameters of the (hexagonal) CEF Hamiltonian. In the ordered state below T_2 (=2.3 K), a large jump in the magnetization takes place around $\mu_0 H$ =0.1 T for fields applied along the $(0,0,L)$ easy magnetic axis. This jump had been interpreted as a spin reorientation.[19] However, the magnetization does not seem to reach saturation even at magnetic fields of 13 T.[20] This finding implies the possible existence of a high-field magnetic structure. Figure 1 depicts the magnetic phase diagram.[27]

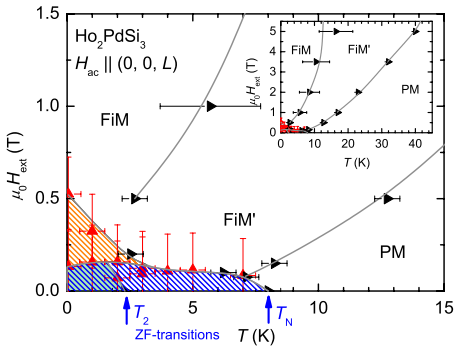

FIG. 1. (Color online) Phase diagram of Ho_2PdSi_3 derived by means of ac susceptibility measured with the external field applied along the $(0,0,L)$ direction. The gray lines are guide to the eyes. The two zero-field transitions are additionally marked. The shaded areas are connected to the low-field structure, the phases marked FiM and FiM′ are attributed to the high-field phase (see text).

The detailed derivation of the phase diagram from ac-susceptibility measurements is described elsewhere.[27] The measurements were made in constant field or constant temperature mode as indicated by the different triangles. The measurements show no differences between up and down field sweeps, i.e., no hysteresis is observed. The transition field related to the large jump in the magnetization is nearly independent of the temperature. Also, below T_2 no apparent change in this behavior is observed and the critical field value of the so-defined H_{c1} can be extrapolated to 0.13 T.

Below T_2 a second phase can be found above H_{c1} and below 0.5 T, the latter defining H_{c2}. The connection between the two transition lines near T_2 is not resolved clearly. In the region below H_{c2} and T_N there exist in total three different magnetic phases as indicated by the different shaded areas in Fig. 1.

Above H_{c2} a large area in the phase diagram is found which contains two more magnetic phases (marked as FiM and FiM′), inferred from faint changes in the field-dependent susceptibility. FiM and FiM′ are separated by a nearly vertical line while the FiM′ to PM phase boundary is a diagonal in the chosen scale within the H-T space. The microscopic difference between FiM and FiM′ is unclear at present. The FiM and FiM′ phases are separated from the paramagnetic region by a line which is shown fully in the inset of Fig. 1. For a magnetic field of 5 T the critical temperature is around 40 K, five times the ordering temperature. As stated above, a transition to the ferromagnetic saturated phase was not observed up to 13 T.

Neutron-diffraction measurements on powder samples were performed earlier by Szytula *et al.*[21] to resolve the magnetic structure in zero field. The magnetic structure of Ho_2PdSi_3 was described as a sinusoidal modulation of magnetic moments aligned along the ***c*** axis with a propagation vector of (0.137, 0.0066, 0) at T=1.5 K. As mentioned earlier, the sinusoidal modulated structure is, in general, not the ground state in rare-earth intermetallic compounds[5,6] and a progressive squaring up comparable to Er_2PdSi_3 (Ref. 22) is expected to occur at T_2. Also a commensurate magnetic structure below T_2 is anticipated.[5]

II. EXPERIMENTAL DETAILS

The neutron-scattering experiments were carried out at the Helmholtz-Zentrum for Materialien und Energie GmbH (formerly Hahn-Meitner Institut) with the E2 diffractometer and at the Laboratoire Léon Brillouin on the 6T2 diffractometer. Additional information, particularly with regard to the magnetic-moment direction, was measured on the PANDA cold triple-axis spectromenter at the Forschungsneutronenquelle Heinz-Maier Leibnitz (FRM-II). On both diffractometers a graphite monochromator with additional pyrolitic graphite filters suppressed the $\lambda/2$ contamination in the incident beam. In all experiments the same Ho_2PdSi_3 single crystal with a mass of 2.9 g was used. The shape of this crystal is slightly irregular with six oriented faces ($\{H,0,0\}$, $\{H,H,0\}$, and $\{0,0,L\}$) ground on a cylindrical sample of 9 mm length and 5 mm diameter. The E2 experiment used a standard-orange-type cryostat capable of reaching 1.5 K base temperature. The wavelength was $\lambda=2.39$ Å. The E2 diffractometer employs a "banana"-type multidetector with 400 channels covering a 2θ angle of 80°. The sample was rotated around the axis perpendicular to the $(H,K,0)$ scattering plane in steps of 0.2°. The result is an ω-2θ map which can be transformed in a full reciprocal plane, easily allowing the search for yet unknown propagation vectors.

The 6T2 experiment ($\lambda=2.345$ Å) employed a ^{3}He-^{4}He-dilution fridge (base temperature below 200 mK) within a vertical magnet. The sample was oriented with its $\boldsymbol{c}$-axis vertical, i.e., along the magnetic field direction. The diffractometer operates with a single detector in normal beam geometry, i.e., a lifting detector arm to allow access out of plane reflections even with a cryomagnet installed. The highest applied field in this experiment was 5 T. The single crystal was mounted inside a specially constructed sample holder filled with a 1:3 mixture of deuterated methanol/ethanol to avoid motion of the sample due to the application of the magnetic field. This mixture freezes in an amorphous phase. As result no background signal from the methanol/ethanol in the investigated $\boldsymbol{Q}$ area was observed. We did not perform a full 2θ scan to fully characterize this special sample holder technique. A subsequent experiment on the 6T2 diffractometer used the (H,H,L) scattering plane with the magnetic field applied parallel to $(H,\bar{H},0)$. In this experiment a standard sample holder and the absence of the dilution fridge resulted in a gain by the factor three of scattered intensity.

The experiment on the PANDA spectrometer used a standard cryostat with a sample temperature of $T=1.4$ K. The $(H,K,0)$ scattering plane geometry was used. The PANDA spectrometer is a classic triple-axis spectrometer at the cold source of the FRM-II. In the case of elastic scattering the used wavelength was 2.36 Å.

Scaling of the intensity

During the 6T2 experiment the performed scans were not ω-2θ rocking scans, but we always employed the UB matrix to go along the $\boldsymbol{Q}$ positions in reciprocal space. The observed integrated intensities depend on the direction of the scans. This was observed during the data evaluation after the experiment. The scale determined for the 1, 0, 0 reflections are $I(L)/I(H)=2.36/1$ and $I(L)/I(HK)=2.65/1$. The reason for the direction dependency of the intensity is the use of only horizontal collimation which leads to higher intensity for the (vertical) L scans. As consequence the width of the reflections scales alike.

A second issue is extinction. Our very large, irregular-shaped single crystal is susceptible for extinction effects, especially when the intensity of a reflection is large. The ferromagnetic ordered magnetic-moment component has been measured on the 1, 0, 0 reflection which has been used also to scale the overall intensity. This reflection gains approximately 13 times in intensity in an applied field of 5 T. The macroscopic measured magnetization,[20] however, suggests the intensity is measured with a factor three too small. Therefore, we tried to model the scaling factor s and extinction factor y. According to the empirical equation[28,29] y can be expressed as $(1+cF^2_{\mathrm{calc}})^{-1/2}$. In general, c is combined from a multitude of parameters (wavelength, sample thickness, etc.). Here, the only changing parameter (for the 1, 0, 0 reflection in dependence of the magnetic field) is the intensity itself and c is constant. The intensity is proportional to the square of the ordered magnetic moment. The expected magnetic structure factor F^2_{calc} of 1, 0, 0 reflection is calculated with the magnetic moment extracted from the measured magnetization. This value is then compared with the observed magnetic structure factor F^2_{obs}. According to $F^2_{\mathrm{obs}}=F^2_{\mathrm{calc}}s(1+cF^2_{\mathrm{calc}})^{-1/2}$ the parameters s and c are then adjusted. In this approach four points were used. The scaling factor s is mostly determined by the zero-field intensity while the extinction parameter replicates the ferromagnetic intensity for 2 T, 3 T, and 5 T. In this field range the change in slope for the macroscopic magnetization is small and the field dependence is approximately linear. The scaling s and extinction parameter c are then applied to correct the intensity of reflections (similar scattering angle) prior to later model calculation.

III. EXPERIMENTAL RESULTS

A. Zero-field structure and its evolution in low fields (<0.8 T)

Figure 2 shows the full reciprocal plane $(H,K,0)$ of Ho_2PdSi_3 at 10 K well above T_N. In the figure the reciprocal vectors (1, 0, 0) and (0, 1, 0) are marked for clarity.

The observed reflections in this plane are the family of symmetrically equivalent {1, 0, 0}, {1, 1, 0}, and {2, 0, 0} on the outer rim of the circle. Scattering on the polycrystalline aluminum of the sample holder and the cryostat yields a faint Debye-Scherrer ring. Additional intensity is found around the {1, 0, 0} reflections in the form of diffuse magnetic intensity due to antiferromagnetic short-range correlations. The center of gravity is $|(1/7,0,0)|$ away from the nuclear reflections. Below T_N magnetic Bragg peaks appear on positions $\{\boldsymbol{G}\pm\boldsymbol{\tau}_0\}$, where $\boldsymbol{G}$ is a reciprocal lattice vector and $\boldsymbol{\tau}_0=(1/7,0,0)$. Further lowering the temperature leads to the progressive appearance of reflections resulting from higher harmonics (odd and even integers) of the propagation vector. Figure 3 shows the reciprocal $(H,K,0)$ plane at $T=1.5$ K. The assumption that the transition at T_2 (~2 K) is equivalent to the squaring up observed in the Er_2PdSi_3 compound[22]

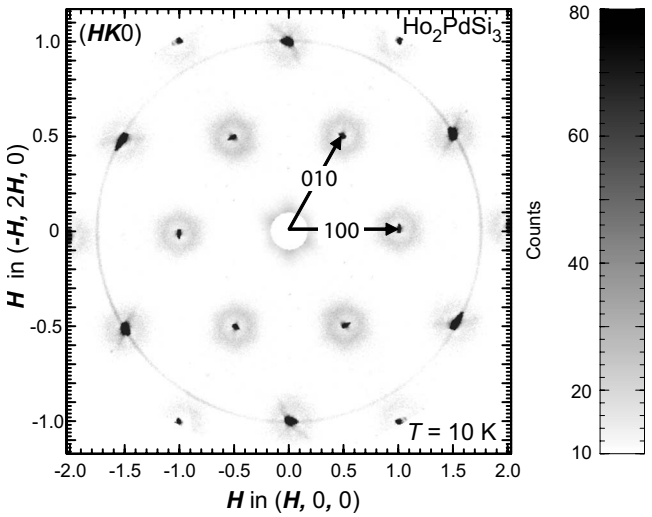

FIG. 2. Full reciprocal $(H,K,0)$ plane of Ho_2PdSi_3 at $T=10$ K. (3 K above the Néel temperature). The reciprocal lattice directions (1, 0, 0) and (0, 1, 0) are marked with arrows. Around the {1, 0, 0} nuclear reflections diffuse magnetic scattering is found with the center of gravity at (1/7, 0, 0). The faint outer ring originates from the scattering on polycrystalline aluminum from the sample holder and the cryostat.

is drawn here. As can be seen already in Fig. 3, the magnetic reflections are split in perpendicular direction to $\boldsymbol{\tau}_0$. The exact propagation vector is therefore $\boldsymbol{\tau}=\boldsymbol{\tau}_0+\boldsymbol{\delta}=(1/7-\delta,2\delta,0)$ with $\boldsymbol{\delta}=(-\delta,2\delta,0)$. The component δ is of order 10^{-3} r.l.u.. No magnetic intensity is found on {1, 0, 0} indicating the lack of a ferromagnetic component in the magnetic structure. This was further verified by the experiment on the PANDA spectrometer, where a set of reflections $\{H,0,L\}\pm\boldsymbol{\tau}$ had been measured. There, the upper limit for a ferromagnetic contribution on {1, 0, 0} was determined to be less than 0.2 μ_B. The magnetic-moment direction can be estimated from the fact that neutrons are only sensitive to the magnetization component perpendicular to the scattering vector $\boldsymbol{Q}$. Figure 4 shows the plot of measured and corrected intensities vs the reciprocal $(H,0,0)$ direction for different values of L. The measured values (bottom) differ in intensity mostly due to the different angle of the magnetization density to the scattering vector. The corrected values (top) have been divided by the square sine of the angle between the scattering vector $\boldsymbol{Q}$ and the $\boldsymbol{c}$ axis. Additionally, the intensity values have been divided by the appropriate magnetic-form factor taken from Ref. 30. The corrected values then match for all L values. The upper limit of the in-plane component of the magnetic moment is less than 0.9 μ_B assuming a structure in which all magnetic moments have their maximum value. Therefore, the main component of magnetic moment in the zero-field magnetic structure is parallel to the $\boldsymbol{c}$ axis.

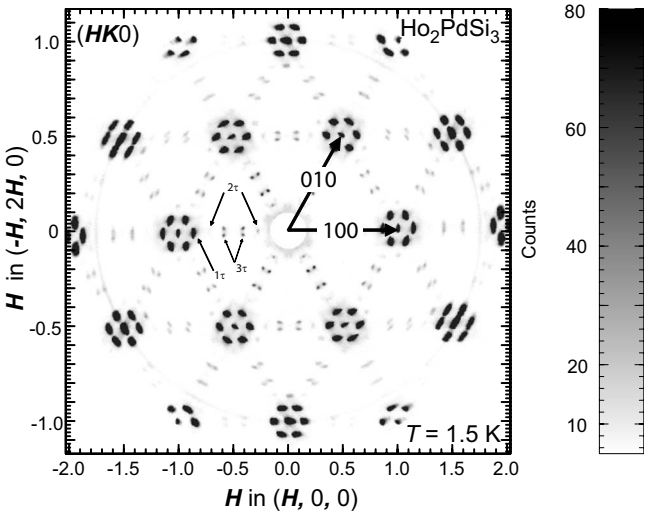

FIG. 3. Full reciprocal $(H,K,0)$ plane of Ho_2PdSi_3 at $T=1.5$ K. The reciprocal lattice directions (1, 0, 0) and (0, 1, 0) are marked with arrows. Magnetic satellites are found around the nuclear positions describable with $\boldsymbol{\tau}=(1/7+\delta,-2\delta,0)$ and its higher harmonics ($2\boldsymbol{\tau}$ and $3\boldsymbol{\tau}$ as indicated). The ring originates from the scattering on polycrystalline aluminum from the sample holder and the cryostat.

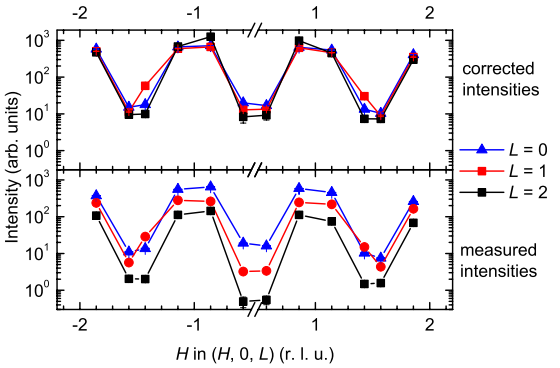

FIG. 4. (Color online) Comparison of the measured (bottom) and corrected (top) intensity of the $\{H,0,L\}\pm\boldsymbol{\tau}$ and $\{H,0,L\}\pm3\boldsymbol{\tau}$ on logarithmic scale. The corrected intensity is divided by the square sine of the angle between the scattering vector $\boldsymbol{Q}$ and the $\boldsymbol{c}$ axis. Additional the form factor (Ref. 30) has been corrected for.

The aim of the experiment on the 6T2 diffractometer in the LLB was to resolve the additional component $\boldsymbol{\delta}$ to understand the mechanism of the spin reorientation and to search for the suspected antiferromagnetic-moment modulation in high (>1 T) fields. The $(H,K,0)$-plane scattering geometry yield the magnetic field direction parallel to $(0,0,L)$. The low temperature, zero-field phase characterized by the propagation vector $\boldsymbol{\tau}=(1/7-\delta,2\delta,0)$ was confirmed at $T=0.187$ K and $\mu_0H=0$ T. The black curve (solid circles) in Fig. 5 shows the $\boldsymbol{Q}$-dependent intensity along the direction $(H,2H,0)$ centered at 2/7, 0, 0. The situation at the magnetic satellite reflection positions is complicated by the fact that, for instance, the intensity around $\boldsymbol{Q}=(2/7,0,0)$ seems to consist of the reflections $2\boldsymbol{\tau}_0\pm\boldsymbol{\delta}$ and $2\boldsymbol{\tau}_0\pm3\boldsymbol{\delta}$. All reflections observed can be indexed with $n\boldsymbol{\tau}_0\pm m\boldsymbol{\delta}$, where n and m are integers. In zero field m takes only odd values.

From zero-field measurements the determination of the transverse component $\boldsymbol{\delta}$ is difficult and cannot be determined unambiguously. When a magnetic field above H_{c1} is applied reflections with $m=2$ are strongly enhanced [compare the red (highest) curve in Fig. 5] allowing an estimation of δ around 0.0055(4) r.l.u. This value can describe all measured magnetic intensity in zero field and applied fields $<H_{c2}$. It is

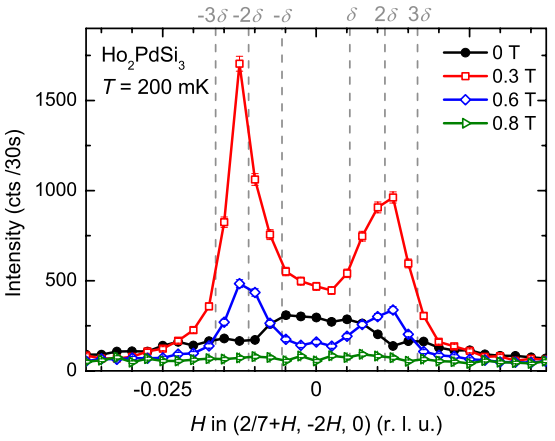

FIG. 5. (Color online) Section along the $(H,2\bar{H},0)$ direction crossing perpendicular to the two $\boldsymbol{\tau}$ magnetic satellites. The measurement is at base temperature (200 mK) with different magnetic fields applied parallel to $(0,0,L)$ as indicated on the top right. The gray lines mark the values for δ and its multitudes (see text for detailed discussion).

worth noting that δ indicates the size of a magnetic unit cell more than 180 times the primitive AlB_2 unit cell. Apparently the transverse component $\boldsymbol{\delta}$ is an essential part of the magnetic structure as it is present up to the critical field where the antiferromagnetic structure is destroyed [around 0.8 T, see the green (lowest) curve in Fig. 5]. Above 0.8 T no antiferromagnetic modulated magnetic intensity is found in the $(H,K,0)$ plane. The difference to H_{c2} determined from the macroscopic measurements (i.e., 0.5 T) may result from the demagnetization factor which is small for the used samples (small oriented rods) compared to the single crystal used for the neutron diffraction. The propagation vector $\boldsymbol{\tau}$ of the zero-field magnetic structure consist of two parts $n\boldsymbol{\tau}_0 \pm m\boldsymbol{\delta}$. At H_{c1} the propagation vector changes slightly with the addition of even values of m while at H_{c2} the zero-field structure is wiped out completely.

Further insight in the zero-field magnetic structure can be gained from measurements in the (H,H,L) scattering geometry where the magnetic field is parallel to $(H,\bar{H},0)$. The magnetic phase diagram for a magnetic field applied in the basal plane shows no transition up to 5 T at $T=2$ K.

In zero field around any nuclear Bragg peak a total of six magnetic reflections with the same intensity due to the first order of the propagation vector $\boldsymbol{\tau}_0$ are observed. The splitting of the first-order magnetic reflections due to the $\boldsymbol{\delta}$ component is too small to be resolved. When a field is applied along $(H,\bar{H},0)$ one propagation vector $\boldsymbol{\tau}_\parallel$ is parallel while $\pm\boldsymbol{\tau}_{a,b}$ have an angle of 60° to the field. With increasing magnetic field the intensity of the reflection due to $\boldsymbol{\tau}_\parallel$ increases while that of the other reflections decreases. At an applied magnetic field of 5 T the magnetic intensity on $\boldsymbol{\tau}_\parallel$ has increased by a factor of three while the intensity of the symmetrical equivalent positions $\boldsymbol{\tau}_{a,b}$ has decreased to zero.

A possible explanation is that the magnetic field depopulates continuously the magnetic domains with the propagation vectors $\boldsymbol{\tau}_{a,b}$ while the domain with $\boldsymbol{\tau}_\parallel$ is populated. At 5 T only the latter remains. The zero-field magnetic structure in Ho_2PdSi_3 is therefore a single-$\boldsymbol{\tau}$, multidomain structure.

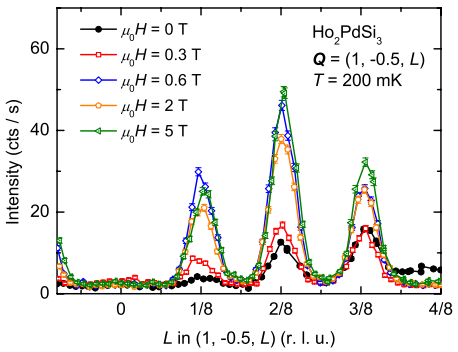

FIG. 6. (Color online) Section along the $(1,-0.5,L)$ direction measured at base temperature (200 mK) with increasing magnetic field [parallel $(0,0,L)$]. The $(1,-0.5,L)$ direction is equivalent to $(0.5,0.5,L)$. The measurement in zero field has been made with a larger incident beam size and has been linearly corrected to equal the background at $L=0$ of the field measurements. The L value in the measurement at 5 T has been corrected with a factor to a smaller lattice constant c.

B. Magnetic structure for higher fields (0.8–5 T)

In applied magnetic fields above H_{c1}, a new magnetic phase yielding reflections on both integer and noninteger positions is found. In both investigated cases [field parallel to $(H,\bar{H},0)$ and $(0,0,L)$, respectively] this new phase was observed. Magnetic intensity was found on the same positions as the crystallographic superstructure reflections. Figure 6 shows the field dependence of the reflections at the 1, −0.5, and $n/8$ positions. The intensity on these positions is not affected by temperature in zero field indicating that the intensity observed on these positions in zero field is of pure nuclear origin. In small magnetic fields at base temperature a large increase in intensity on these positions is observed. Figure 7 shows the integrated intensity of the three reflections. The magnetic intensity vs field plot shows maxima for the three reflections around 0.6 T. For fields above 0.6 T the magnetic intensity at first decreases but then increases with increasing field leading to a shallow minimum at 2 T. The

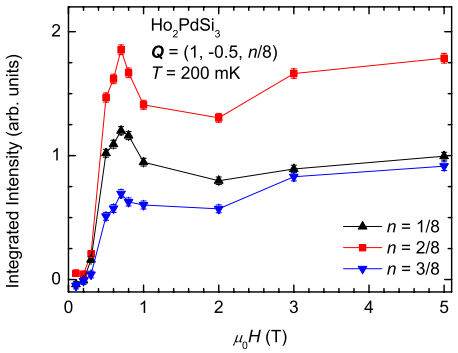

FIG. 7. (Color online) Integrated intensities of the reflections shown in Fig. 6 vs magnetic field. The field is along $(0,0,L)$ and the temperature is 200 mK. The nuclear contribution measured at zero field is subtracted.

increase in intensity with increasing field is observed up to the highest measured field of 5 T.

In contrast with the more complicated, nonmonotonic field dependence of the magnetic satellite, the increase in the ferromagnetic intensity on, e.g., the 1, 0, 0 reflection is, in general, agreement with the observed macroscopic magnetization from Ref. 20. Again, the differences between macroscopic and microscopic data can be understood if different demagnetization factors are considered.

IV. DISCUSSION

A. Zero-field magnetic structure

In zero field and below T_2, the simple sine-modulated structure model which has been derived from powder measurements[21] is in disagreement with our observation of the higher harmonics which imply a squared-up structure. However, a full squared-up modulation with a propagation of only $\boldsymbol{\tau}_0=(1/7,0,0)$ cannot be realized without a ferromagnetic component which seems to be absent (within an error of 0.2 μ_B) both in powder and single-crystal data. Possibilities for the magnetic structure are therefore either a modulation of the magnetic moments, a noncollinear structure or an additional compensation of the net magnetic moment generated by a squared-up structure. The modulation of the magnetic moments is contradicted by the appearance of the higher harmonics. The noncollinear possibility is excluded since the moments appear to be parallel to the $\boldsymbol{c}$ axis. Additionally, group-theory analysis eliminates the possibility to have a small in-plane component of the propagation vector $\boldsymbol{\tau}$. Under the $P6/mmm$ symmetry group of the crystal structure, the little group of the propagation vector $\boldsymbol{\tau}$ is $\mathbb{G}^{\tau 1}=\{1,m_{xy0}\}$. The irreducible representations (Ireps) of the little group are $\Gamma 1$ and $\Gamma 2$. The combination of the magnetic and permutation representation contains one time Ireps $\Gamma 1$ and two times $\Gamma 2$. The associated basis functions of the irreducible representations are $(0,0,\mu_z)$ for $\Gamma 1$ and $(\mu_x,\mu_y,0)$ for $\Gamma 2$. Therefore, the spontaneous magnetic order with a propagation vector $\boldsymbol{\tau}$ as allowed by symmetry has a moment either parallel to the $\boldsymbol{c}$ axis or in the $\boldsymbol{ab}$ plane. As shown earlier the main component of the magnetic component is parallel to the $\boldsymbol{c}$ direction. If the $P6/mmm$ symmetry is preserved for the zero-field structure, then the magnetic structure should be described by $\Gamma 1$ Ireps with the absence of an in-plane component of the magnetic moment.

In an equal-moment structure, the magnetic moments are squared up in both directions $(H,0,0)$ and $(H,2\bar{H},0)$. The sequence of 4+ and 3− is then reversed after $2/\boldsymbol{\delta}$. The net magnetic moment per unit cell is then compensated to zero over the spin sequence defined by the perpendicular component the propagation vector. The modulation of the magnetic moment can be described as $\boldsymbol{\mu}(\boldsymbol{R})=\Sigma_{n,m}\boldsymbol{\mu}(n\boldsymbol{\tau}_0)\cdot\boldsymbol{\mu}(m\boldsymbol{\delta})\cdot e^{(n\boldsymbol{\tau}_0+m\boldsymbol{\delta})\cdot\boldsymbol{R}}$. Figure 8 shows a sketch of the proposed structure. The spin sequence is somehow related to a "spin-slip" structure and is possible favored energywise by the absence of a ferromagnetic stray field. In zero magnetic field only the odd multitudes of $\boldsymbol{\delta}$ seem present indicating the absence of a ferromagnetic component. In applied field also the even multitudes are observed. The appearance of the even harmonics is accompanied with the increase in the ferromagnetic component. The magnetic structure above H_{c1} is describable with the same formalism as the zero-field structure.

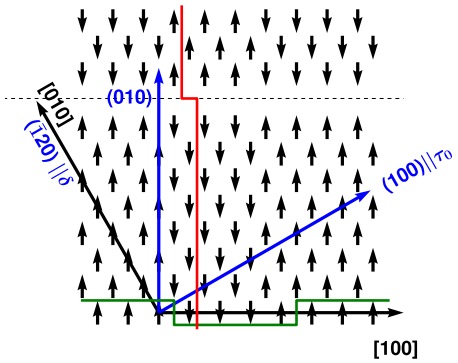

FIG. 8. (Color online) Sketch of the zero-field magnetic structure of Ho_2PdSi_3. The magnetic moments point in $(0,0,L)$ direction (perpendicular to the drawing plane). They are squared up in both directions as indicated by the red (vertical) and green (horizontal) lines. The [100] and [010] are the directions in real space while the (100) and $(\bar{1}20)$ directions are in the reciprocal space. The dashed line in the middle denotes the many rows of magnetic moments omitted in the drawing.

The observations in an applied magnetic field perpendicular to the $\boldsymbol{c}$ axis, i.e., in the basal plane comply with the proposed model. The magnetic field changes only the population of the domains in the favor of the domain with the propagation vector component $\boldsymbol{\tau}_0$ parallel to the field. The cause of this is still unclear. In all magnetic domains the magnetic moments are perpendicular to the applied field and therefore the Zeeman term is equal. A possible explanation can be anisotropic dipole-dipole exchange.

The model of the zero-field magnetic structure is still rather speculative and realistic calculations are difficult because of the very large magnetic unit cell and the large number of free parameters overshadowing the amount of experimental information.

B. High-field magnetic structure

For the high-field structure calculations are easier to perform since the number of magnetic moments involved is "only" 4×8 resulting from the 2×2 enlarged basal plane and the octuplication along the $\boldsymbol{c}$ direction. Still, the number of free parameters is much higher than the number of observations making assumptions necessary. The calculation has been done for the data set measured when the magnetic field was applied parallel $(0,0,L)$. The modeling of the case field parallel $(H,\bar{H},0)$ is similar.

Two models are considered possible and will be discussed in the following. Both of them consider the two local environments for the Ho^{3+} sites as reason for the observed magnetic structures. The difference between both models is whether exchange interaction (model 1) or the local CEF (model 2) is dominant. In the former the RKKY exchange

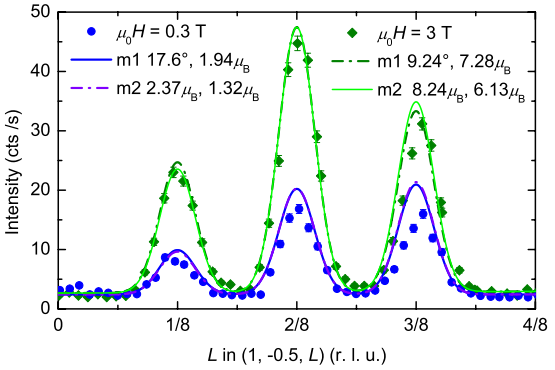

FIG. 9. (Color online) Comparison of the model calculations with the experiment [field parallel $(0,0,L)$]. The nuclear contribution and a constant background are added to the model calculation. The abbreviations m1 and m2 stand for model one and two (see text). The 2/8 reflection has been used for the fitting and the differences between both scenarios can therefore be seen only on the 1/8 and 3/8 reflections.

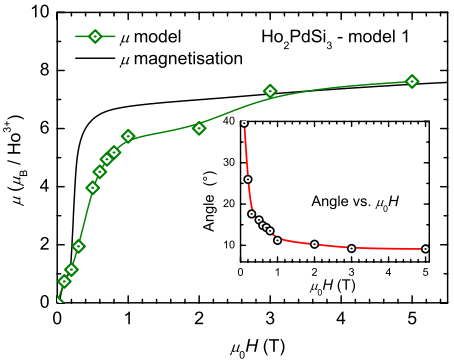

FIG. 10. (Color online) Magnetic field dependence [field parallel $(0,0,L)$] for the two parameters of scenario one: magnetic moment and angle (inset). The lines are guide to the eyes. The black line shows the field dependence of the macroscopic magnetization measured on a different single crystal with smaller demagnetization field.

interaction is modulated by the Pd-Si order while in the latter the CEF effect leads to different magnetic ground states of the Ho^{3+} ion for the two different sites.

The first model considers equal magnetic moments which are coupled via an exchange interaction mediated by the conduction electrons (RKKY). The conduction-electron density and therefore the exchange interaction acting on the Ho^{3+} is modulated by the Pd-Si order. The observed effects are ascribed by competition between exchange interactions and the Zeeman and the magnetocrystalline anisotropy term. The equal ordered moments form a structure consisting of eight layers stacked in the $\boldsymbol{c}$ direction. Each layer has a ferromagnetic component of the magnetic moment parallel to the $\boldsymbol{c}$ direction. In the case of exchange interaction, the magnetic-moment direction is canted away from the $\boldsymbol{c}$ axis. This angle varies in applied fields from 40° to 9°. The magnetic-moment component in the basal plane has to be strict antiferromagnetic to comply with the measured reflections. The direction of the magnetic moment in the plane can be chosen freely under the assumption that at least a threefold symmetry is conserved. The intensity variations will then be balanced by the contributions from the different domains (equal population assumed). This simple model uses the collinear antiferromagnetic sequence ++−−−++− along the $\boldsymbol{c}$ axis for the moment component in the basal plane while the moment component parallel $(0,0,L)$ is ferromagnetic. This sequence corresponds to the sequence of the different rare-earth sites ($R1$-$R2$-⋯). The moments are antiferromagnetically arranged along the $(H,0,0)$ direction. The results of this model are compared to the experimental data and are shown in Fig. 9 for two representative fields. The nice feature on this model is that only two parameters are left free: the magnitude of magnetic moment and the angle of magnetic moment with respect to the $\boldsymbol{c}$ axis. The ferromagnetic intensity is mostly affected by the magnitude of the magnetic moment while the intensity on top of the superstructure reflections is mostly affected by the angle of the magnetic moment toward the $\boldsymbol{c}$ axis. Since the relative intensity between the harmonics of the propagation vector changes only slightly as a function of field the whole intensity vs field relation can be modeled. This is visualized in Fig. 10 where the magnitude of the magnetic moment and the angle (inset) is shown. In applied fields the angle rapidly decreases as the magnetic moments are forced to orient parallel to the $\boldsymbol{c}$ axis. Above H_{c2} this trend continues but the rate of decrease in applied magnetic fields is reduced gradually. For comparison the macroscopic magnetization from Ref. 20 is also plotted in Fig. 10.

In the second model the local-site symmetry results in two different CEF ground states for the Ho^{3+} ion, resulting in different magnetic moments for each site. The exchange interaction is in this model only responsible for the zero-field magnetic structure. The exchange is weak so that a small external field (<0.8 T) is sufficient to override it and all observed effects in applied fields result from the two different magnetic moments. The difference between the two Ho^{3+} sites gives rise to two different CEF states. Thus varies their response to the external field. As a consequence of crystallographic superstructure, a magnetic unit cell of the size $2\times2\times8$ results. Eight layers are stacked along the $\boldsymbol{c}$ axis with four magnetic moments of different value (μ_1 and μ_2) in each layer. The stacking sequence (μ_1-μ_2-⋯) on the four positions in each layer is the same as used in the model presented before (replacing "+" with μ_1 and "−" with μ_2). Applying a field along $\boldsymbol{c}$ axis, both moments try to align to the field, however, the magnitude of the moments change with different rate. Over the whole field range the magnitude of both moments increases. The behavior of the two magnetic moments is shown in Fig. 11.

Shown in Fig. 9 are the calculations for the 0.3 and 3 T data with μ_1=2.37 μ_B and μ_2=1.32 μ_B for 0.3 T and μ_1=8.24 μ_B and μ_2=6.13 μ_B for 3 T. With this model one can explain the increase in the AFM intensity with the increase in field, namely, Fig. 7. The data from calculation is very close to measurement. It is worth mentioning that this model does not rule out the possibility of any AFM ordering in the plane. They might be as well present considering the missing moment from the saturation.

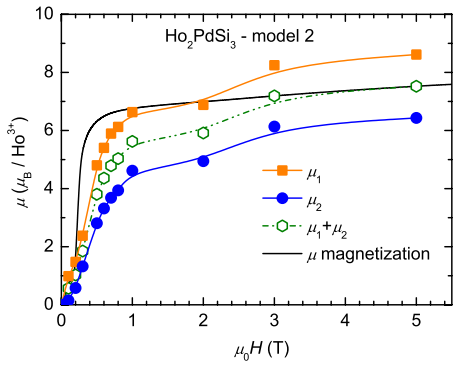

FIG. 11. (Color online) Magnetic field dependence [field parallel $(0,0,L)$] of the two different magnetic moments of scenario two (solid symbols). Additionally, the averaged moment and the macroscopic magnetization are plotted. The lines are guide to the eyes.

V. CONCLUSION

Summarizing, the magnetic structure of single-crystalline Ho_2PdSi_3 has been investigated in a detailed neutron-diffraction study with temperatures down to 200 mK and applied magnetic fields up to 5 T. The observed magnetic structures imply a delicate balance between RKKY exchange interaction, crystal electric field, the frustration of nearest-neighbor interaction on the triangular lattice and the two different local environments of the Ho^{3+} ion due to the formation of a Pd-Si order.

The zero-field magnetic structure was investigated and the propagation vector could be identified to $\boldsymbol{\tau}=(1/7-\delta,2\delta,0)$, where δ is around 0.0055(4) r.l.u., with the help of a small applied magnetic field. The magnetic structure in Ho_2PdSi_3 is a single-$\boldsymbol{\tau}$, multidomain structure with the magnetic-moment direction mainly along the $\boldsymbol{c}$ direction. Our results clarify the previously reported magnetic structure: the magnetic structure is not sinusoidal modulated but rather a squared-up modulated structure. The squared-up structure points to an equal-moment structure. Both facts can be understood in comparison to other rare-earth intermetallic compounds.[5] The propagation vector has two components. The 1/7 modulation is commensurate within the experimental error while the $\boldsymbol{\delta}$ component seems to belong to an incommensurate modulation superimposed on the commensurate modulation. In our approaches we could not calculate intensities for the zero-field magnetic structure but outlined a possible model. The sequence of 4+ and 3− of the model is consistent with predictions for a 1/7 modulation[4] but allows furthermore for the fact that the magnetic structure of Ho_2PdSi_3 seems to be the realization of a *commensurate, long-period, equal moment, squared-up*, and *compensated* magnetic structure. The zero-field magnetic structure is independent from the observed crystallographic superstructure.

The existence of a ferrimagnetic (FiM) structure in applied fields (above 0.8 T) has been proposed and could be identified within this work. Two possible models have been evaluated but cannot be distinguished with the present data set. Further measurements are needed to clarify this issue. For instance, the measurement of angular-dependent magnetization could identify an easy magnetic direction at an angle from the main crystallographic directions which is needed for the first model. Another possibility is to measure a magnetic contribution of the FiM phase on the 0, 0, 1 reflection which is proposed to be zero by the second model. However, to measure this reflection a horizontal magnet with the magnetic field in the *HHL* scattering plane is needed.

The most elegant way is to search for a high-field magnetic structure in Gd_2PdSi_3. If found, the high-field magnetic structure is due to the exchange interaction since the crystal electric field effect does not exist for Gd^{3+} (*S*-state ion). The necessary neutron and magnetic x-ray scattering experiments in applied fields on a Gd_2PdSi_3 single crystal are planned.

The spin sequence which both models use to describe the antiferromagnetic structure in applied fields is unique in respect to the experimental data. No other spin sequence can be constructed to model the distinctive reflection pattern. Though the presented two models for the high-field magnetic structure are not definite and the real magnetic structure may even be a combination of both, the spin sequence $(++--++-)$ is unambiguously established. The spin sequence is equal to the sequence of the rare-earth ions given by the nuclear superstructure.

Both, the existence of the crystallographic superstructure and the high-field antiferromagnetic phase are indicated for most of the R_2PdSi_3 with heavy rare earths (R=Gd-Tm). The finding of a high-field magnetic structure modulated by the crystallographic superstructure in Ho_2PdSi_3 might be key to understand the magnetic properties of other R_2PdSi_3 compounds in applied magnetic fields. The high-field magnetic structure is the result of a field-induced interplay between crystallographic and magnetic structures. The situation that the magnetic structure in the ground state seems to be unaffected by this interplay but the structure in applied field is effectively mirroring the crystallographic superstructure is without precedence.

ACKNOWLEDGMENTS

We acknowledge the technical and scientific support from the staff at the neutron scattering centers Helmholtz-Zentrum for Materialien und Energie GmbH, Laboratoire Léon Brillouin, and Forschungsneutronenquelle Heinz-Maier Leibniz (FRM-II). The Ho_2PdSi_3 single crystal was grown in the Leibniz Institute for Solid State and Materials Research Dresden by H. Bitterlich and W. Loeser. One author (M.F.) acknowledges the sponsorship of this research at Oak Ridge National Laboratory's Spallation Neutron Source by the Scientific User Facilities Division, Office of Basic Energy Sciences, U.S. Department of Energy.

*Corresponding author; frontzekmd@ornl.gov

[1] J. Jensen and A. R. Mackintosh, *Rare Earth Magnetism* (Clarendon Press, Oxford, 1991).
[2] D. Gignoux and D. Schmitt, *Handbook of Magnetic Materials* (Elsevier Science B. V., 1997), Vol. 10, Chap. 2, pp. 239–413.
[3] P. Bak and J. von Boehm, Phys. Rev. B **21**, 5297 (1980).
[4] D. Gignoux and D. Schmitt, Phys. Rev. B **48**, 12682 (1993).
[5] D. Gignoux and D. Schmitt, J. Magn. Magn. Mater. **100**, 99 (1991).
[6] R. J. Eliott, Phys. Rev. **124**, 346 (1961).
[7] D. Gignoux, D. Schmitt, A. Takeuchi, and F. Y. Zhang, J. Magn. Magn. Mater. **97**, 15 (1991).
[8] V. Sima, Z. Smetana, B. Lebech, and E. Gratz, J. Magn. Magn. Mater. **54-57**, 1357 (1986).
[9] F. Steglich, C. D. Bredl, M. Loewenhaupt, and K. D. Schotte, J. Phys. Colloq. **C5-40**, 301 (1979).
[10] J. Schweizer, F. Givord, J.-X. Boucherle, F. Bourdarot, and E. Ressouche, J. Phys.: Condens. Matter **20**, 135204 (2008).
[11] A. B. Harris and J. Schweizer, Phys. Rev. B **74**, 134411 (2006).
[12] P. A. Kotsanidis, J. K. Yakinthos, and E. Gamari-Seale, J. Magn. Magn. Mater. **87**, 199 (1990).
[13] G. Graw, H. Bitterlich, W. Löser, G. Behr, J. Fink, and L. Schultz, J. Alloys Compd. **308**, 193 (2000).
[14] I. Mazilu, M. Frontzek, W. Löser, G. Behr, A. Teresiak, and L. Schultz, J. Cryst. Growth **275**, e103 (2005).
[15] S. Majumdar, E. V. Sampathkumaran, P. L. Paulose, H. Bitterlich, W. Löser, and G. Behr, Phys. Rev. B **62**, 14207 (2000).
[16] P. L. Paulose, E. V. Sampathkumaran, H. Bitterlich, G. Behr, and W. Löser, Phys. Rev. B **67**, 212401 (2003).
[17] K. Iyer, P. L. Paulose, E. V. Sampathkumaran, M. Frontzek, A. Kreyssig, M. Doerr, M. Loewenhaupt, I. Mazilu, W. Löser, and G. Behr, Physica B **355**, 158 (2005).
[18] S. R. Saha, H. Sugawara, T. D. Matsuda, H. Sato, R. Mallik, and E. V. Sampathkumaran, Phys. Rev. B **60**, 12162 (1999).
[19] E. V. Sampathkumaran, H. Bitterlich, K. K. Iyer, W. Löser, and G. Behr, Phys. Rev. B **66**, 052409 (2002).
[20] M. Frontzek, A. Kreyssig, M. Doerr, M. Rotter, G. Behr, W. Löser, I. Mazilu, and M. Loewenhaupt, J. Magn. Magn. Mater. **301**, 398 (2006).
[21] A. Szytula, M. Hofmann, B. Penc, M. Ślaski, S. Majumdar, E. V. Sampathkumaran, and A. Zygmunt, J. Magn. Magn. Mater. **202**, 365 (1999).
[22] M. Frontzek, A. Kreyssig, M. Doerr, A. Schneidewind, J.-U. Hoffman, and M. Loewenhaupt, J. Phys.: Condens. Matter **19**, 145276 (2007).
[23] A. R. Ball, D. Gignoux, and D. Schmitt, J. Magn. Magn. Mater. **119**, 96 (1993).
[24] M. Frontzek, A. Kreyssig, M. Doerr, J.-U. Hoffman, D. Hohlwein, H. Bitterlich, G. Behr, and M. Loewenhaupt, Physica B **350**, E187 (2004).
[25] F. Tang *et al.* (unpublished).
[26] S. R. Saha, H. Sugawara, T. D. Matsuda, Y. Aoki, H. Sato, and E. V. Sampathkumaran, Phys. Rev. B **62**, 425 (2000).
[27] M. Frontzek, Dissertation, Cuvillier Verlag Goettingen, 2009.
[28] W. H. Zachariasen, Acta Crystallogr. **23**, 558 (1967).
[29] P. J. Becker and P. Coppens, Acta Crystallogr., Sect. A: Cryst. Phys., Diffr., Theor. Gen. Crystallogr. **30**, 129 (1974).
[30] A. J. Freeman and J. P. Desclaux, J. Magn. Magn. Mater. **12**, 11 (1979).